The rise of oxygen-driven arsenic cycling at ca. 2.48 Ga

Ernest Chi Fru[1], Andrea Somogyi[2], Abderrazzak El Albani[3], Kadda Medjoubi[2], Jérémie Aubineau[3], Leslie J. Robbins[4], Stefan V. Lalonde[5], and Kurt O. Konhauser[4]

[1]Centre for Geobiology and Geochemistry, School of Earth and Ocean Sciences, College of Physical Sciences and Engineering, Cardiff University, Cardiff CF10 3AT, Wales, UK

[2]Nanoscopium beamline, Synchrotron SOLEIL, L'Orme des Merisiers Saint-Aubin, BP 48, 91192 Gif-sur-Yvette Cedex, France

[3]Institut de Chimie des Milieux et Matériaux de Poitiers, UMR 7285–CNRS, Université de Poitiers, 5 rue Albert Turpin (Bât B35), 86073 Poitiers cedex, France

[4]Department of Earth and Atmospheric Sciences, University of Alberta, Edmonton, Alberta T6G 2E3, Canada

[5]Laboratoire Géosciences Océan, CNRS-UMR6538, European Institute for Marine Studies, Université de Bretagne Occidentale, 29280 Plouzané, France

ABSTRACT

The Great Oxidation Event (GOE) at 2.45 Ga facilitated the global expansion of oxidized compounds in seawater. Here, we demonstrate that the GOE coincided with a sharp increase in arsenate and arsenic sulfides in marine shales. The dramatic rise of these oxygen-sensitive tracers overlaps with the expansion of key arsenic oxidants, including oxygen, nitrate, and Mn(IV) oxides. The increase in arsenic sulfides by at least an order of magnitude after 2.45 Ga is consistent with the proposed transition to mid-depth continental-margin sulfide-rich waters following the GOE. At the same time, the strong increase in arsenate content, to ~60% of the total arsenic concentration in shales, suggests that the oxidative component of the arsenic cycle was established for the first time in Earth's history. These data highlight the global emergence of a new selective pressure on the survival of marine microbial communities across the GOE, the widespread appearance of toxic, oxidized chemical species such as arsenate in seawater.

INTRODUCTION

The Great Oxidation Event (GOE) marks a pivotal point in Earth's history, when appreciable amounts of O_2 first permanently accumulated in the atmosphere (Lyons et al., 2014). This rise in atmospheric O_2 allowed shallow surface seawater to become globally oxygenated, while sulfide-rich conditions developed in middle-depth continental-margin waters and anoxic iron-rich conditions persisted at depth (Poulton and Canfield, 2011). Abundant mineralogical and geochemical evidence support the timing of the GOE, including the disappearance of detrital pyrite, uraninite, and siderite from fluvial and deltaic deposits, an increase in Fe retention in paleosols, chromium (Cr) and uranium (U) enrichments in iron formations and marine shales, and perhaps most importantly, the disappearance of sedimentary sulfur (S)–isotope mass-independent (S-MIF) anomalies (see Farquhar et al. [2011] and Lyons et al. [2014] for reviews).

With the onset of oxidative weathering, seawater would have been supplied with increased amounts of oxidized species, such as arsenate, As(V), the oxidized form of arsenic (As). With an arsenite [As(III)] As(III)/As(V) redox potential close to that of Fe(II)/Fe(III) and NO_3^-/N_2^- (O'Day, 2006), As(V) should have formed readily during the GOE. This would have been amplified by the accumulation of oxidized compounds such as NO_3^- and Mn(IV) oxides that, in turn, serve as As(III) oxidants (see Oremland and Stolz, 2003; see also the GSA Data Repository[1]). Once formed, As(V) could have been reduced back to As(III) in either the water column or sediment pile after interacting with electron donors like H_2S and organic carbon.

Whether on land, in the oceans, or in Earth's subsurface and surface environments, the redox cycling of As follows a simple pathway, determined chiefly by the presence or absence of oxygen and sulfide (Smedley and Kinniburgh, 2002; O'Day et al., 2004; O'Day, 2006). Based on this conservative behavior of the As cycle in nature, we posit that the abundances of As(V) and As sulfides (As-S) in Precambrian marine shales should effectively track As speciation and accumulation in the oxic and sulfide-rich environments that became widespread following the rise of atmospheric oxygen.

METHODS

Drill-core shale samples, aged ca. 2.7–2.0 Ga, are from near-continental-margin deposits associated with biological activity (Table DR1; Bekker et al., 2004; Canfield et al., 2013; Martin et al., 2015; Chi Fru et al., 2015, 2016a). X-ray absorption near edge spectroscopy (XANES) was performed to evaluate the As speciation (see supplementary methods in the Data Repository). To account for variation in speciation for a given sample, location, or geological age, each sample was measured between five and 60 times. Major elements were measured by inductively coupled plasma–atomic emission spectrometry (ICP-AES), and trace elements by ICP–mass spectrometry (ICP-MS) and ICP–optical emission spectrometry (ICP-OES) as previously described (Ngombi-Pemba et al., 2014; Chi Fru et al., 2015). Ferric iron oxide (Fe_2O_3) was determined as the difference between total iron [$(Fe_2O_3)_T$] and ferrous iron (FeO). FeO was quantified by titration. Banded iron formation data assembled from a literature survey and new chemical analyses are detailed in Table DR2 and supplementary methods in the Data Repository.

RESULTS

We sampled marine shales from 39 deposits across 10 nearshore marine successions formed between ca. 2.7 and 2.0 Ga (Table DR1 in the Data Repository). Essentially, the sample suite was chosen based on previous studies demonstrating their usefulness as proxies for Precambrian seawater and atmospheric composition because of limited post-depositional modification (Canfield et al., 2013; Chi Fru et al., 2015, 2016a; see supplementary methods in the Data Repository). These, together with ~800 iron formation samples spanning ca. 3.8 Ga to present, were analyzed for

As, Ti, and Fe content (Table DR2). The oxidation state of As and associated elements in shale minerals was examined by X-ray absorption near edge spectroscopy (XANES) (Fig. DR1 in the Data Repository) and X-ray fluorescence (Fig. DR2), respectively. After we excluded potential X-ray–induced oxidation of reduced As(III) species to As(V), and As(V) reduction during XANES analysis, our data revealed the following:

(1) Early Paleoproterozoic shale As/Fe ratios are mostly within the Neoarchean range, rising from a minimum of ~1.0×10^{-6} at the Archean-Proterozoic boundary to a maximum of 4.0 at ca. 2.0 Ga (Fig. 1A).

(2) With the exception of one sample, As(III) was exclusively below the XANES detection limit (Table DR1), implying that <15% of total As might be present as As(III). XANES spectra exhibit two prominent peaks in the 11.8695–11.8705 keV range, corresponding to As-S and As(V) species (Fig. DR1).

(3) The gradual increase in total As content in marine sediments across the GOE is mainly due to As-S and As(V) enrichment (Figs. 1B–1C).

(4) As-S and As(V) enrichment begins at 2.48 Ga, intensifying in the 2.32 Ga Timeball Hill Formation, South Africa (Fig. 1C), consistent with previously reported Cr and U enrichments in iron formations (Konhauser et al., 2011; Partin et al., 2013).

(5) As/Ti ratios in iron formations coincide with an increase in the oxidative supply of As from land to the oceans at the GOE (Fig. 2A). A lack of strong variability in As/Fe ratios across the GOE transition (Fig. 2B) suggests that the size of the Fe pool was not a major determinant of sediment As concentration and speciation trends at this time.

(6) In the Francevillian shales, Gabon, bulk As concentrations >50 ppm increase with rising Fe-oxide content (Fig. DR3A). However, there is a generally weak correlation between Fe-oxide and As concentration across the Francevillian Series. This is most prominent when As is <50 ppm (Fig. DR3A), along with a correlation between Mo and As in the sulfide-rich FD formation of the Francevillian Series (Figs. DR4 and DR5). This suggests that the rise of near–continental margin sulfidic conditions across the GOE was a critical factor controlling sediment As content and oxidation state.

(7) Some Precambrian pyrite-specific As enrichments are significant (Large et al., 2014; Gregory et al., 2015), but may not represent bulk shale As concentrations (Figs. DR3B and DR3C).

DISCUSSION

The similar range of As/Fe ratios recorded during the early Paleoproterozoic relative to the Archean in both shales and iron formations suggests that the rise of As(V) and As-S species across the GOE cannot be explained by rapid fluctuations in the sedimentary Fe reservoir (see the Data Repository). Instead we suggest that this change is linked to the intensification of oxidative
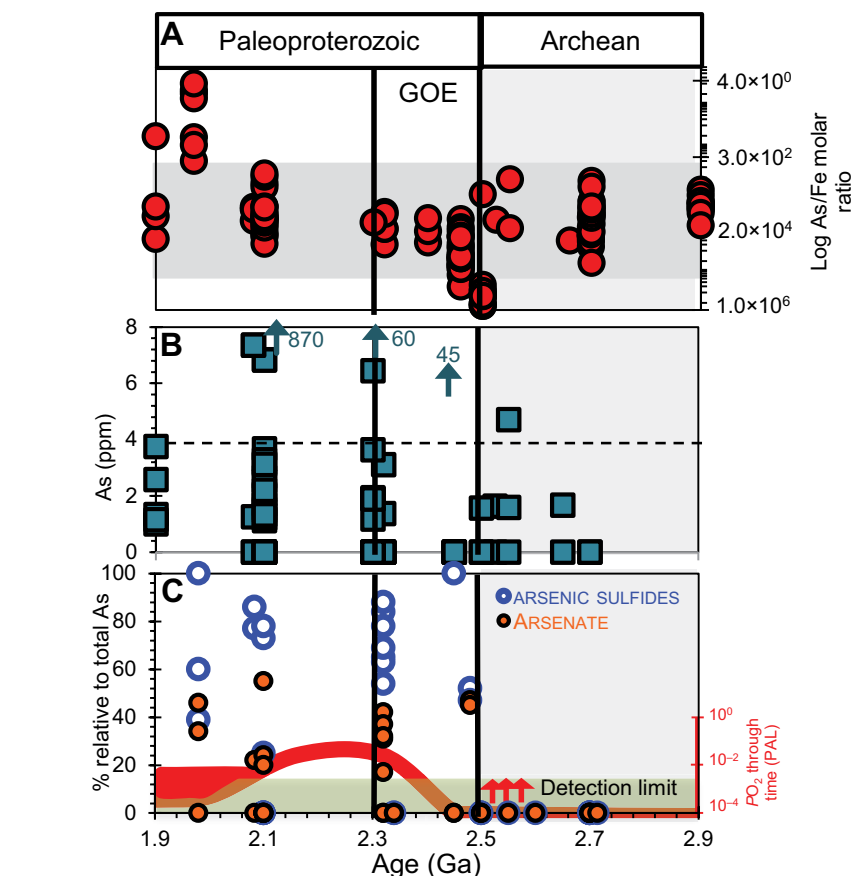

Figure 1. Secular sedimentary arsenic (As) dynamics across Archean-Proterozoic boundary. A: Bulk As/Fe ratio trends (see Chi Fru et al. [2015] for data description). Horizontal shading indicates range of Archean values. B: Bulk average As content in shales across sampled interval measured by inductively coupled plasma–optical emission spectrometry. Arrows are maximum X-ray fluorescence values (see Methods in text and Table DR1 [see footnote 1]). C: X-ray absorption near edge spectroscopy (XANES) data showing distribution of As species in shales. Red trace line shows atmospheric oxygenation dynamics relative to present atmospheric level (PAL), according to Lyons et al. (2014). Red arrows show whiffs of O_2 according to Anbar et al. (2007). Green shading indicates XANES detection limit, which is 15% total As content; data below detection limit are statistically uncertain and are rounded down to zero for graphical display. GOE—Great Oxidation Event.

weathering of a felsic and/or As-S–rich continental crust (Konhauser et al., 2011; Large et al., 2018; see the Data Repository for details), containing up to 1500 ppm of As (Henke, 2009). The peak in As/Ti ratios in iron formations at ca. 2.48 Ga is consistent with a contemporaneous spike in Cr/Ti ratios, interpreted to reflect the onset of terrestrial aerobic sulfide oxidation (Konhauser et al., 2011). The muted GOE iron formation As/Fe signal, relative to Archean ratios, and the knife-sharp rise in the As/Ti trend across the GOE (Fig. 2A) may be related to Snowball Earth glaciations influencing continental As supply patterns (Chi Fru et al., 2015). This hypothesis is supported by the suppression of As/Fe and As/Ti ratios in Neoproterozoic iron formations (Figs. 2A and 2B; Table DR2) that are a product of submarine hydrothermal activity and a result of ice sheets restricting sediment supply and promoting water-column anoxia (Hoffman et al., 1998; see the Data Repository).

Under anoxic conditions, As and S chemistry becomes coupled, such that sulfide production scales with As-S deposition (O'Day et al., 2004; Data Repository). Arsenic sulfides, however, can be oxidized to As(V) in O_2-rich conditions (e.g., the case of arsenopyrite in Reaction 1).

$$4FeAsS + 13O_2 + 6H_2O \rightarrow \\ 4H_3As_4 + 4FeSO_4. \quad (1)$$
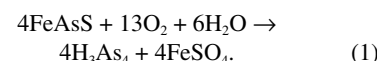
In addition, the formation of As(V) only occurs when relevant As(III) oxidants (e.g., O_2, MnO_2, NO_3^-) are available (Oremland and Stolz, 2003; see the Data Repository). Electron donors are required to regenerate As(III) from As(V), and as today, microbes catalyze both the oxidative and reductive reactions (Oremland and Stolz, 2003). As(V) accumulation, therefore, occurs when production rates are greater than consumption rates, likely explaining the observed rise of As(V) in the data:

Anoxygenic photosynthetic and anoxic NO_3^--dependent chemoautotrophic oxidation of As(III) have been proposed as the most viable mechanisms by which appreciable Archean As(V) production could have occurred (Oremland and Stolz, 2003; Sforna et al., 2014). If these processes were prominent over As(V) reduction,
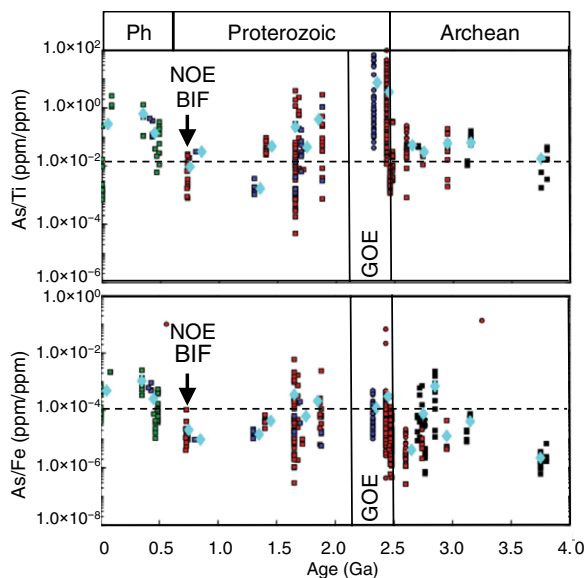
Figure 2. Distribution of As in iron formations (IFs), spread through Earth's history. A: As/Ti ratio. B: As/Fe ratio. Red symbols are Superior-type IFs; black, Algoma-type IFs; blue, ironstones; and green, Phanerozoic hydrothermal iron sediments. Squares represent bulk sample digestions; circles, laser ablation analyses. Light blue diamonds show 100 m.y. time-binned averages, plotted in middle of each bin (e.g., 2.4–2.5 Ga, plotted at 2.45 Ga). Two bins, plotted at 3.25 Ga and 0.55 Ga, were excluded from As/Fe plot as they were represented by single sample each. Ph—Phanerozoic; GOE—Great Oxidation Event.
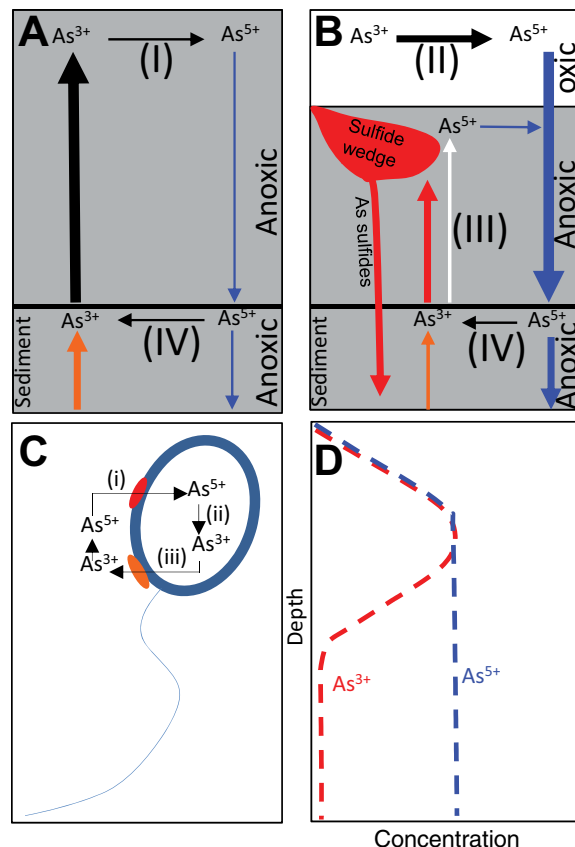
a strong sedimentary As(V) signal would be expected. Our data, however, suggest that anoxic As(III) oxidation of Archean crust was limited, relative to that of post-GOE deposits. To this end, there is a significant increase in As(V) in the 2.32 Ga Timeball Hill Formation, suggesting that As(V) production outpaced consumption, compared to the period before. Further, the prevalence of As-S coincides with significant pyrite deposition in Timeball Hill black shales (Bekker et al., 2004). The strength and reproducibility of the As-S and As(V) signals (Fig. 1C) are consistent with the oxidation of terrestrial minerals containing reduced As to produce soluble As(V) that was then transported to the oceans during the GOE.

In addition to being a strong As(III) oxidant, O_2, as it accumulated in the atmosphere, would have initiated the generation of additional As(III) oxidants, including Mn(IV) oxides and NO_3^- (Oremland and Stolz, 2003; Roy, 2006; Zerkle et al., 2017). As expected, the elevated As-S content in shales coincides with the suggested expansion of microbial reduction of sulfate, coincident with the GOE (Kah et al., 2004; Poulton and Canfield, 2011; Planavsky et al., 2012). Neither diagenesis nor the photochemical oxidation of As are likely to have significantly affected our interpretation (see the Data Repository).

Major biogeochemical As cycling pathways in the anoxic Archean oceans are proposed to have been distinct from those operating in the redox-stratified Paleoproterozoic seawater column (Figs. 3A and 3B). Accordingly, the oxidative supply of As(V) from land promotes the large-scale uptake of As(V) through phosphate transporters by marine phytoplankton. This is followed by intracellular As(V) reduction via cytoplasmic As(V)-reductases and the extrusion of As(III) by membrane transporters (Fig. 3C) (Dyhrman and Haley, 2011; Wurl et al., 2013, 2015; Yan et al., 2014; Sánchez-Riego et al., 2014; Saunders and Rocap, 2016). The conversion of As(V) to As(III) minimizes phosphate loss, as physicochemical similarities between As(V) and phosphate complicates differentiation by the cell. Not surprisingly, As(V) displays nutrient-like behavior in the modern oxidized ocean, with a rapid increase in the thermocline and near-constant concentration at depth (Cutter and Cutter, 2006; Wurl et al., 2013, 2015). The shuttling of As(V) into, and As(III) out of, the cell followed by rapid re-oxidation back to As(V) limits As sedimentation and increases seawater residence time (Henke, 2009). This thermodynamic disequilibrium accounts for up to 20% of inorganic As in the oxygenated surface ocean being present as As(III) (Cutter et al., 2001; Cutter and Cutter, 2006; Wurl et al., 2013, 2015; Fig. 3D).

Importantly, some oxidized compounds mobilized for the first time during the GOE would have been toxic for microbes that had evolved in their absence under dominantly anoxic marine conditions. Arsenate, for instance, is toxic to all three domains of life down to the nanomolar range and its concentration displays a strong inverse relationship with marine primary production, particularly because of the interference of As(V) with phosphate metabolism (see Smedley and Kinniburgh, 2002; Dyhrman and Haley, 2011; see the Data Repository). Methylated arsenicals, implicated in the adaptation of early life to As-rich environments (Chen et al., 2017) and linked to As detoxification, contain ≥35% of As in the photic zone (Cutter et al., 2001; Cutter and Cutter, 2006; Wurl et al., 2013, 2015). This biological processing of As, plus sulfide and Fe(III)-(oxyhydr)oxide mineralization, would have influenced the distribution of As resistance, As-based metabolisms, and biological phosphate uptake in extant biota (see the Data Repository for a discussion on implications for biological arsenic cycling and phosphate uptake). It has also been suggested that the large-scale deposition of iron formations at the Archean-Paleoproterozoic transition facilitated the preferential incorporation of phosphorus (P) over As(V) into Fe(III) (oxyhydr)oxides. This

Figure 3. Conceptual models of principal marine arsenic (As) cycling pathways. A: Proposed Archean As cycle. B: Proposed Paleoproterozoic As cycle. (I)—potential predominant anoxygenic photosynthetic oxidation of As(III) to As(V) in unstratified Archean oceans with low sulfide content; (II)—potential elevation of As(III) oxidation to As(V) in Great Oxidation Event (GOE) redox stratified oceans, coupled to rise in seawater oxygen, Mn-oxide, and sulfate content; (III)—potential decrease in As-dependent anoxygenic photoautotrophy and increase in chemoautotrophic nitrate-dependent oxidation of As(III) to As(V) after GOE; (IV)—As(III) regeneration by anaerobic dissimilatory As(V) reduction with organic matter. White, blue, red, and orange arrows represent As(III) regenerated in sediments and water column through anaerobic As(V) reduction, As(V) production by As(III) oxidation, As-sulfide formation pathways, and hydrothermal As(III) release, respectively. Arrow size represents hypothesized size of pool for each As species reaction pathway. C: A microbial cell performing As(V) detoxification: (i)—phosphate transporter (red); (ii)—cytoplasmic As(V) reduction to As(III); (iii)—extrusion of As(III) through As(III) efflux pump (orange). D: Conceptual model depicting behavior of As(III) and As(V) in modern fully oxygenated ocean (Cutter et al., 2001; Maher and Butler, 1988).

would have led to a simultaneous buildup of As(V) and depletion of P in seawater that would have negatively impacted marine primary productivity (Chi Fru et al., 2016b; Hemmingsson et al., 2018).

The rise in As-S and As(V) appears some 30 m.y. before the loss of S-MIF, providing compelling evidence that the GOE was protracted rather than instantaneous. This rise in marine As-S and As(V) across the Archean-Proterozoic boundary overlaps with the expansion of major As oxidants during the GOE. We propose that this radical change enabled the expansion of a global As cycle reminiscent of the modern, and is related to the onset of abundant As-S and As(V) species in sulfidic and oxygenated environments, respectively. The emergence and impact of these toxic species have yet to be considered despite this knowledge forming a critical prerequisite for understanding how life adapted to the new redox landscape that emerged with the GOE.

REFERENCES CITED
Anbar, A.D., et al., 2007, A whiff of oxygen before the Great Oxidation Event?: Science, v. 317, p. 1903–1906, https://doi.org/10.1126/science.1140325.

Bekker, A., Holland, H.D., Wang, P.-L., Rumble, D., Stein, H.J., Hannah, J.L., Coetzee, L.L., and Beukes, N.J., 2004, Dating the rise of atmospheric oxygen: Nature, v. 427, p. 117–120, https://doi.org /10.1038/nature02260.

Canfield, D.E., et al., 2013, Oxygen dynamics in the aftermath of the Great Oxidation of Earth's atmosphere: Proceedings of the National Academy of Sciences of the United States of America, v. 110, p. 16,736–16,741, https://doi.org/10.1073/pnas .1315570110.

Chi Fru, E., Arvestål, E., Callac, N., El Albani, A., Kilias, S., Argyraki, A., and Jakobsson, M., 2015, Arsenic stress after the Proterozoic glaciations: Scientific Reports, v. 5, 17789, https://doi.org/10 .1038/srep17789.

Chi Fru, E., Rodríguez, N.P., Partin, C.A., Lalonde, S.V., Andersson, P., Weiss, D.J., El Albani, A., Rodushkin, I., and Konhauser, K.O., 2016a, Cu isotopes in marine black shales record the Great Oxidation Event: Proceedings of the National Academy of Sciences of the United States of America, v. 113, p. 4941–4946, https://doi.org/10 .1073/pnas.1523544113.

Chi Fru, E., Hemmingsson, C., Holm, M., Chiu, B., and Iñiguez, E., 2016b, Arsenic-induced phosphate limitation under experimental Early Proterozoic oceanic conditions: Earth and Planetary Science Letters, v. 434, p. 52–63, https://doi.org/10.1016 /j.epsl.2015.11.009.

Chen, S.-C., Sun, G.-X., Rosen, B.P., Zhang, S.-Y., Deng, Y., Zhu, B.-K., Rensing, C., and Zhu, Y., 2017, Recurrent horizontal transfer of arsenite methyltransferase genes facilitated adaptation of life to arsenic: Scientific Reports, v. 7, 7741, https://doi.org/10.1038/s41598-017-08313-2.

Cutter, G.A., and Cutter, L.S., 2006, Biogeochemistry of arsenic and antimony in the North Pacific Ocean: Geochemistry Geophysics Geosystems, v. 7, Q05M08, https://doi.org/10.1029 /2005GC001159.

Cutter, G.A., Cutter, L.S., Featherstone, A.M., and Lohrenz, S.E., 2001, Antimony and arsenic biogeochemistry in the western Atlantic Ocean: Deep-Sea Research Part II: Topical Studies in Oceanography, v. 48, p. 2895–2915, https://doi.org/10.1016 /S0967-0645(01)00023-6.

Dyhrman, S.T., and Haley, S.T., 2011, Arsenate resistance in the unicellular marine diazotroph Crocosphaera watsonii: Frontiers in Microbiology, v. 2, 214, https://doi.org/10.3389/fmicb.2011.00214.

Farquhar, J., Zerkle, A.L., and Bekker, A., 2011, Geological constraints on the origin of oxygenic photosynthesis: Photosynthesis Research, v. 107, p. 11–36, https://doi.org/10.1007/s11120-010-9594-0.

Gregory, D., et al., 2015, Trace element content of sedimentary pyrite in black shales: Economic Geology and the Bulletin of the Society of Economic Geologists, v. 110, p. 1389–1410, https://doi.org /10.2113/econgeo.110.6.1389.

Hemmingsson, C., Pitcain, I.K., and Chi Fru, E., 2018, Evaluation of uptake mechanisms of phosphate by Fe(III) (oxyhydr)oxides in early Proterozoic oceanic conditions: Environmental Chemistry, v. 15, p. 18–28, https://doi.org/10.1071/EN17124.

Henke, K.V., ed., 2009, Arsenic: Environmental Chemistry, Health Threats and Waste Treatment: West Sussex, UK, John Wiley and Sons, 588 p., https:// doi.org/10.1002/9780470741122.

Hoffman, P.F., Kaufman, A.J., Halverson, G.P., and Schrag, D.P., 1998, The Neoproterozoic snowball Earth: Science, v. 281, p. 1342–1346, https://doi .org/10.1126/science.281.5381.1342.

Kah, C.L., Lyons, T.W., and Frank, T.D., 2004, Low marine sulphate and protracted oxygenation of the Proterozoic biosphere: Nature, v. 431, p. 834–838, https://doi.org/10.1038/nature02974.

Konhauser, K.O., et al., 2011, Aerobic bacterial pyrite oxidation and acid rock drainage during the Great Oxidation Event: Nature, v. 478, p. 369–373, https://doi.org/10.1038/nature10511.

Large, R., et al., 2014, Trace element content of sedimentary pyrite as a new proxy for deep-time ocean-atmosphere evolution: Earth and Planetary Science Letters, v. 389, p. 209–220, https://doi.org /10.1016/j.epsl.2013.12.020.

Large, P.R., Mukherjee, I., Zhukova, I., Cockrey, R., Stepanov, A., and Danyushevsky, L.V., 2018, Role of upper-most crustal composition in the evolution of the Precambrian ocean-atmosphere system: Earth and Planetary Science Letters, v. 487, p. 44–53, https://doi.org/10.1016/j.epsl.2018.01.019.

Lyons, T.W., Reinhard, C.T., and Planavsky, N.J., 2014, The rise of oxygen in Earth's early ocean and atmosphere: Nature, v. 506, p. 307–315, https://doi .org/10.1038/nature13068.

Maher, W., and Butler, E., 1988, Arsenic in the marine environment: Applied Organic Chemistry, v. 2, p. 191–214, https://doi.org/10.1002/aoc .590020302.

Martin, A.P., Prave, A.R., Condon, D.J., Lepland, A., Fallick, A.E., Romashkin, A.E., Medvedev, P.V., and Rychanchik, D.V., 2015, Multiple Palaeoproterozoic carbon burial episodes and excursions: Earth and Planetary Science Letters, v. 424, p. 226–236, https://doi.org/10.1016/j.epsl.2015.05.023.

Ngombi-Pemba, L., El Albani, A., Meunier, A., Grauby, O., and Gauthier-Lafaye, F., 2014, From detrital heritage to diagenetic transformations, the message of clay minerals contained within shales of the Palaeoproterozoic Francevillian basin (Gabon): Precambrian Research, v. 255, p. 63–76, https://doi .org/10.1016/j.precamres.2014.09.016.

O'Day, P.A., 2006, Chemistry and mineralogy of arsenic: Elements, v. 2, p. 77–83, https://doi.org/10 .2113/gselements.2.2.77.

O'Day, P.A., Vlassopoulos, D., Root, R., and Rivera, N., 2004, The influence of sulfur and iron on dissolved arsenic concentrations in the shallow subsurface under changing redox conditions: Proceedings of the National Academy of Sciences of the United States of America, v. 101, p. 13,703–13,708, https://doi.org/10.1073/pnas.0402775101.

Oremland, R.S., and Stolz, J.F., 2003, The ecology of arsenic: Science, v. 300, p. 939–944, https://doi .org/10.1126/science.1081903.

Partin, C.A., Lalonde, S.V., Planavsky, N.J., Bekker, A., Rouxel, O.J., Lyons, T.W., and Konhauser, K.O., 2013, Uranium in iron formations and the rise of atmospheric oxygen: Chemical Geology, v. 362, p. 82–90, https://doi.org/10.1016/j.chemgeo.2013 .09.005.

Planavsky, N.J., Bekker, A., Hofmann, A., Owens, J.D., and Lyons, T.W., 2012, Sulfur record of rising and falling marine oxygen and sulfate levels during the Lomagundi event: Proceedings of the National Academy of Sciences of the United States of America, v. 109, p. 18,300–18,305, https://doi .org/10.1073/pnas.1120387109.

Poulton, S.W., and Canfield, D.E., 2011, Ferruginous conditions: A dominant feature of the ocean through Earth's history: Elements, v. 7, p. 107–112, https://doi.org/10.2113/gselements.7.2.107.

Roy, S., 2006, Sedimentary manganese metallogenesis in response to the evolution of the Earth system: Earth-Science Reviews, v. 77, p. 273–305, https:// doi.org/10.1016/j.earscirev.2006.03.004.

Sánchez-Riego, A.M., López-Maury, L., and Florencio, F.J., 2014, Genomic responses to arsenic in the cyanobacterium Synechocystis sp. PCC 6803: PLoS One, v. 9, e96826, https://doi.org/10.1371 /journal.pone.0096826.

Saunders, J.K., and Rocap, G., 2016, Genomic potential for arsenic efflux and methylation varies among global Prochlorococcus populations: The ISME Journal, v. 10, p. 197–209, https://doi.org/10.1038 /ismej.2015.85.

Sforna, M.C., Philippot, P., Somogyi, A., van Zuilen, M.A., Medjoubi, K., Schoepp-Cathenet, B., Nitschke, W., and Visscher, P.T., 2014, Evidence for arsenic metabolism and cycling by microorganisms 2.7 billion years ago: Nature Geoscience, v. 7, p. 811–815, https://doi.org/10.1038/ngeo2276.

Smedley, P.L., and Kinniburgh, D.G., 2002, A review of the source, behaviour and distribution of arsenic in natural waters: Applied Geochemistry, v. 17, p. 517–568, https://doi.org/10.1016/S0883-2927 (02)00018-5.

Wurl, O., Zimmer, L., and Cutter, G.A., 2013, Arsenic and phosphorus biogeochemistry in the ocean: Arsenic species as proxies for P-limitation: Limnology and Oceanography, v. 58, p. 729–740, https:// doi.org/10.4319/lo.2013.58.2.0729.

Wurl, O., Shelley, R.U., Landing, W.M., and Cutter, G.A., 2015, Biogeochemistry of dissolved arsenic in the temperate to tropical North Atlantic Ocean: Deep-Sea Research Part II: Topical Studies in Oceanography, v. 116, p. 240–250, https://doi.org /10.1016/j.dsr2.2014.11.008.

Yan, C., Wang, Z., and Luo, Z., 2014, Arsenic efflux from Microcystis aeroginosa under different phosphate regimes: PLoS One, v. 9, e116099, https:// doi.org/10.1371/journal.pone.0116099.

Zerkle, A.L., Poulton, S.W., Newton, R.J., Mettam, C., Claire, M.W., Bekker, A., and Junium, C.K., 2017, Onset of the aerobic nitrogen cycle after the Great Oxidation Event: Nature, v. 542, p. 465–467, https://doi.org/10.1038/nature20826.

Printed in USA